Received: 11 July 2023 | Revised: 25 April 2024 | Accepted: 2 May 2024

DOI: 10.1002/jbm.a.37737

TECHNICAL NOTE

Society For Biomaterials | WILEY

Comparing fabrication techniques for engineered cardiac tissue

Rachel Hatano[1] | Ariell M. Smith[2] | Ritu Raman[3,4] | Jose E. Zamora[5] | Rashid Bashir[4] | Kara E. McCloskey[1,6]

[1]Graduate Program in Bioengineering and Small-scale Technologies, University of California, Merced, USA

[2]Bioengineering Department, University of California, Merced, USA

[3]Department of Mechanical Engineering, Massachusetts Institute of Technology, Cambridge, USA

[4]Department of Bioengineering, University of Illinois at Urbana-Champaign, Urbana, USA

[5]Graduate Program in Materials and Biomaterials Science and Engineering, University of California, Merced, USA

[6]Materials Science and Engineering Department, University of California, Merced, USA

Correspondence
Kara E. McCloskey, School of Engineering, University of California, Merced, 5200 N. Lake Rd., Merced 95343, CA, USA.
Email: kmccloskey@ucmerced.edu

Funding information
This work was funded through the NSF-Science and Technology Center (STC) for the Emergent Behavior of Integrated Biological Systems (EBICS) Award # 0939511; NSF-Science and Technology Center, Grant/Award Number: 0939511

Abstract

Tissue engineering can provide in vitro models for drug testing, disease modeling, and perhaps someday, tissue/organ replacements. For building 3D heart tissue, the alignment of cardiac cells or cardiomyocytes (CMs) is important in generating a synchronously contracting tissue. To that end, researchers have generated several fabrication methods for building heart tissue, but direct comparisons of pros and cons using the same cell source is lacking. Here, we derived cardiomyocytes (CMs) from human induced pluripotent stem cells (hiPSCs) and compare the assembly of these cells using three fabrication methods: cardiospheres, muscle rings, and muscle strips. All three protocols successfully generated compacted tissue comprised of hiPSC-derived CMs stable for at least 2 weeks. The percentage of aligned cells was greatest in the muscle strip (55%) and the muscle ring (50%) compared with the relatively unaligned cardiospheres (35%). The iPSC-derived CMs within the muscle strip also exhibited the greatest elongation, with elongation factor at 2.0 compared with 1.5 for the muscle ring and 1.2 for the cardiospheres. This is the first direct comparison of various fabrication techniques using the same cell source.

KEYWORDS
cardiomyocytes, cardiosphere, cell alignment, cell assembly, muscle strip, pluripotent stem cells, tissue engineering

1 | INTRODUCTION

The field of tissue engineering has inspired researchers to re-imagine, design, and construct microphysiological systems as in vitro organ models of development and disease. While drug discovery has historically relied on 2D cell culture and animal models, the low predictive power of these models is burdening the industry—with only one in 10 drugs making the leap from phase I clinical trial to FDA approval.[1] What's more, the therapeutic potential of pharmaceuticals is limited in tissues that have little-to-no regenerative capabilities. The research and clinical relevance of engineered tissues is only valuable to the extent at which the cellular microenvironment and architecture accurately represents in vivo tissue. As 3D engineered tissues and organ-on-a-chip technologies are better able to recapitulate human physiology, their promise as effective tools in drug development and/or replacement tissue therapy approaches reality.[2,3]

Cell organization within tissues plays a critical role in cell growth, death, migration,[4] as well as cell-to-cell communication and electrical propagation.[5] The relationship between cell organization and cell/tissue function has been shown in the visual cortex,[6] granulosa cells,[7] mammary cells,[8] stem cells,[9] and cardiomyocytes.[10] Moreover, cell patterning in organs can lead to highly complex configurations such as gut undulation,[11] neural circuits,[12] or angiogenesis and vasculogenesis.[13]

For building heart tissue, the alignment of cardiac cells or cardiomyocytes (CMs) is important in generating a synchronously contracting tissue. CM alignment enhances the maturation of β-adrenoreceptor signaling,[14] calcium cycling,[15,16] and force generation.[15,17] Mathematical models of collagen alignment in the heart corroborate increased left ventricular stroke volume with increased cell alignment.[18] Topographical guidance of cardiac cells on patterned surfaces has been shown to enhance alignment, cell–cell communication, and contractile forces of the cardiac cells.[19]

The three major tissue engineering techniques for generating engineered heart tissue (EHT) involve cell-hydrogels, cellularization of acellularized or preformed matrix, and layering cell-sheets. Our laboratory has explored the generation of topographically-aligned CM sheets and found that cell sheets of single cell layers can be generated using topographically-guided CM alignment,[20] but highly contractile sticky CM cell sheets resist stacking into larger structures.[21] Acellularized matrix[22] can preserve native 3-D architecture and vascularity but is not yet able to integrate high densities of cells. As such, the hydrogel technique is considered the most promising method for creating functional myocardium with high cell densities and flexible designs such that heart muscles develop within devices[23] and maintain geometrical forms[24] allowing attachment to force transducers. The hydrogel technique can include mechanically active strip-like muscles[25] cast into molds in which two flexible silicone posts are positioned from above.[26] The posts allow the tissue to be mechanically strained for enhancing cell alignment and contractile forces.[27]

Current methods for fabricating 3D heart tissue[28] include: micro-engineered hydrogels,[29] cardiac biowires,[30] cardiac muscle strips,[31] as well as, unaligned 3D cardiospheres.[32] However, because these studies were conducted in different laboratories using a range of cell sources: skeletal muscle cells, neonatal or mature primary rat or mouse cardiac cells, or stem cell-derived cardiomyocytes, comparing the pros and cons of these distinct fabrication methods is difficult.

Here, we derive reproducible CM cell populations from human induced pluripotent stem cells (hiPSCs) and compare the cardiac tissue assembly of these cells using three distinct methods: generation of cardiospheres,[32,33] assembly of muscle rings using a ring-shaped mold,[34] and formation of muscle strips using a sacrificial gelatin template[35] (Figure 1). We then compared the cell compaction, alignment and elongation within these tissues. The results show that the increased cell alignment and elongation is best achieved using the muscle strip assembly.

2 | MATERIALS AND METHODS

2.1 | Maintenance of human iPS cells

DF 19–9-7 T human induced pluripotent cells (hiPSCs; WiCell) with puromycin under α-MHC (donated by Dr. Chiamvimonvat, UC Davis)[36,37] were plated on Human Embryonic Stem Cell-Qualified Matrigel™-coated dishes (Corning), and fed mTeSR Medium (STEMCELL Technologies, Inc.) daily. Cultures were passed at 80% confluence by dissociating the colonies for 3 min with Accutase (Innovative Cell Technologies). Cell pellets were re-suspended in mTeSR Medium and re-plated onto Human Embryonic Stem Cell-Qualified Matrigel™-coated dishes diluted per manufacturer specifications.

2.2 | Cardiomyocyte differentiation

Cardiomyocytes were generated using a previously published protocol.[38] Briefly, hiPSCs were prepared by dissociating with Accutase (STEM CELL Technologies, Inc), plated at 5×10^5 cells per well in hESC-Qualified Matrigel™-coated 12-well dishes, treated with 5 μM Rho-associated, coiled-coil containing protein kinase inhibitor (ROCKi, Y27632; Selleckchem), and fed 2 mL of mTeSR™1 Medium every day for 4 days (days −4 to −1). On the first day of induction (day 0), cells were re-plated in Roswell Park Memorial Institute (RPMI; Thermo

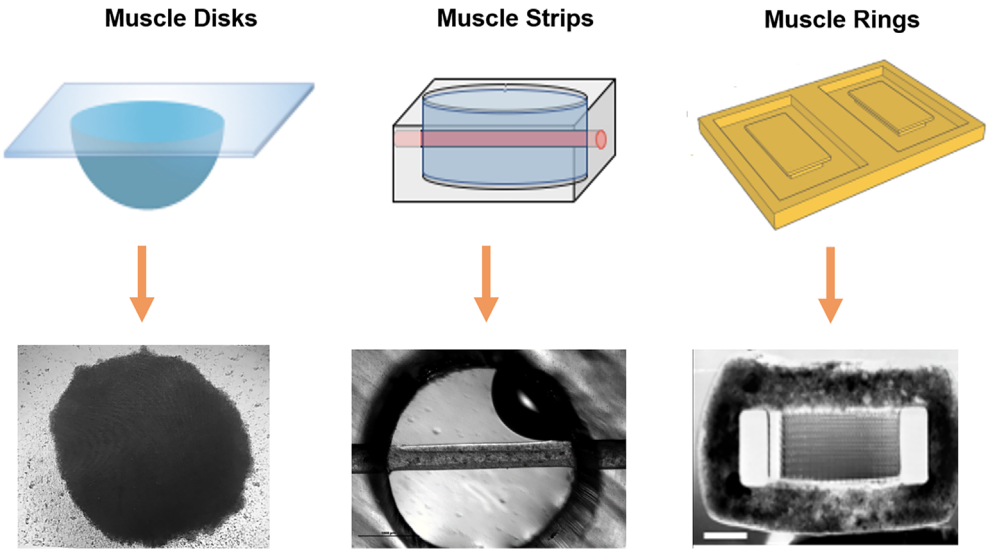

FIGURE 1 Photographs of the three methods used to generate 3D muscle: cardiospheres, muscle strips, and muscle rings. The top images include schematics of the lab-on-chip platforms used for forming the muscle tissues. The bottom images depict the hiPSC-derived CMs after self-assembly within each platform.

Fisher Scientific) supplemented with 2 mL of 2% B27 without insulin (Thermo Fisher Scientific) and 12 μM of GSK-3B inhibitor (CHIR99021; Tocris). After 24 h, the medium was replaced with 2 mL of RPMI/B27 medium without insulin or GSK-3 inhibitor. On day 3, a partial medium change was completed with 1 mL of fresh RPMI/B27 without insulin and supplemented with 5 mM Wnt inhibitor (IWP-2; Tocris) to the 2 mL volume. On day 5, cells were fed with fresh RPMI/B27 without insulin. Starting on day 7, cells were fed with RPMI/B27 with insulin every other day. After 21 days, the hiPSC-derived CMs were purified with 3.6 μg/mL puromycin (Thermo Fisher Scientific) treatment for 24 h and fed with RPMI/B27 every 3 days. Purified hiPSC-derived CMs were harvested between days 24 and 40.

2.3 | Immunostaining for fluorescence microscopy

For staining, the cells were first washed with PBS, fixed via 4% (v/v) paraformaldehyde for 15 min at room temperature. The staining solution consisted of 5% (w/v) nonfat dry milk, 0.4% (v/v) Triton X-100 in PBS, and either Oct-3/4 (eBioscience) pluripotent marker, or α-actinin (Santa Cruz Biotech). Cells were incubated in the staining solution for 1 h at room temperature before undergoing three PBS washes and DAPI counter-staining for 5 min. For cytoskeletal organization of human iPSC-derived CMs, cells were stained and observed under fluorescence microscopy 24 h after seeding (day 24 of total differentiation). Images were taken using a Nikon microscope.

2.4 | Immunostaining for flow cytometry

Cell purities were determined using fluorescence activated cell scanning. Cells were washed with PBS, then dissociated by incubating with 0.25% trypsin for 5 min at 37°C. Single cell suspensions were achieved by washing and pipetting each dish with cell culture medium. After pelleting, the cells were resuspended in 1% (v/v) formaldehyde in PBS for 20 min at room temperature followed by 90% (v/v) cold methanol and incubated for 15 min at 4°C. After fixation, the cells were counted using a hemocytometer and split into tubes containing 0.5 million cells in 2 mL of PBS buffer with 1% Bovine Serum Albumin, washed twice, and stained in 100 μL of flow buffer with either Oct-3/4 (eBioscience), or cardiac troponin T (Thermoscientific). Stained cells were then washed and resuspended in 2 mL of flow buffer and transferred to a round bottom flow tube. Sorting was run on BD LSRII flow cytometer.

3 | QUANTIFICATION OF CARDIOMYOCYTE BEAT RATE

Beat rates were collected as the number of contractions per minute, or beats per minute (bpm), determined by visually using live or recorded videos and counting the number of contractions each cell ($N = 100$) for 1 min each.

3.1 | Generation of 3D cardiospheres

Cell aggregates containing approximately 1×10^6 hiPSC-CMs each were formed by passing and suspending hiPSC-CMs in RPMI with 20% FBS (Thermo Fisher Scientific). Using a multichannel pipette, 50 μL of solution was dropped onto the lid of a 150 mm cell culture dish. The lid was inverted and incubated in 37°C and 5% CO^2 for 12 h to allow the cells to aggregate at the bottom of the droplet. It should be noted that although co-cultures of CMs with of non-myocytes (fibroblasts, endothelial cells and smooth muscle cells) appear to improve tissue architecture and the cardiomyocyte phenotype,[39,40] we used only pure CMs in order to maintain continuity across 3D tissue platforms.

3.2 | Generation of 3D muscle ring

Molds used to generate 3D muscle rings were fabricated by collaborator, Rashid Bashir, University of Illinois, Urbana-Champaign (Figure 2). Using a stereolithographic 3D printer (SLA 250/50, 3D Systems), an ultraviolet laser (325 nm) selectively polymerized a photosensitive hydrogel resin comprised of 20% wt/v poly (ethylene glycol) diacrylate (PEGDA;1000 g/mol) with 0.5% wt/v biocompatible photoinitiator Irgacure 2959.[41] Once completed, the molds were transported in PBS and sterilized by soaking in 70% ethanol for 30 min and rinsed with sterile PBS for an additional 45 min. To generate the 3D muscle tissue, 300 μL solution of 1% NaOH (Millipore Sigma), 200 NHI units of thrombin (Millipore Sigma), 30% v/v Matrigel™ (Corning), 5 mg/mL fibrinogen (Millipore Sigma), and cell culture medium containing 1 mg/mL aminocaproic acid (Millipore Sigma) with 10 million cells/mL was

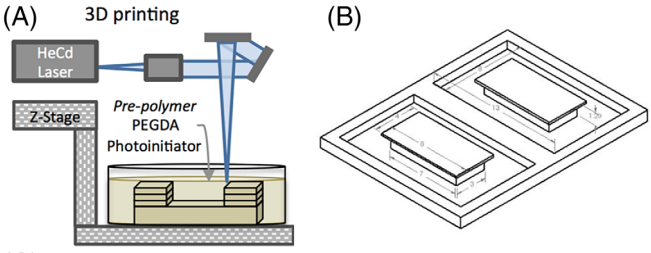

(C)

2 rings	Component %	Volume = 300μL
NaOH	1% v/v	3μL
Thrombin	5 NIHunits/mL	7.5μL
Matrigel	30%	90μL
Fibrinogen	5mg/mL	150μL (of 10mg/mL stock)
cells	20x10^6 cells/mL	6x10^6 cells in 49.5μL

FIGURE 2 Fabrication of muscle ring. (A) Schematic of steriolithographic 3D printing the ring mold. (B) This design is 15 × 20 mm total and supports two muscle rings. (C) In order to make 2 rings, 150 μL of solution is added to each ring mold containing thrombin, fibrinogen, NaOH, Matrigel, and 6 million hiPSC-derived CMs was added to the ring mold.

pipetted into the cavity of the ring mold. After 20 min at 37°C, additional cell culture medium containing 1 mg/mL aminocaproic acid (Millipore Sigma) was gently added to fill the 35 mm petri dish. Media was replaced every other day.

3.3 | Generation of 3D muscle strip

The protocol for muscle strip assembly has been previously developed.[31] Briefly, a 10:1 ratio of PDMS and curing agent was de-gassed, poured on a 3D printed mold with 0.5 mm music wire inserted through the mold holes. After solidifying at 60°C for 2 h, the music wire and PDMS were removed from the mold. To make individual devices, a razor blade can be used to cut through the PDMS between the hollowed-out channels. Three cavities were carved and discarded using a 6 mm biopsy punch. After inserting two music wires with a diameter of 0.5 mm through the device cavities, the PDMS was plasma treated and bonded to a glass coverslip.

Tissue was created (Figure 3) by allowing a solution of 10% (w/v) gelatin (Millipore Sigma), 1% (v/v) NaOH (Millipore Sigma), and 300 NHI units of thrombin (Millipore Sigma) form around the 0.5 mm diameter wire or 6 mm O-rings. After 45 min at 4°C to allow the solution to solidify, the wire or O-ring was removed. A solution of 5 mg/mL fibrinogen (Millipore Sigma), 10% v/v Matrigel™, 20 million cells/mL, and RPMI with 20% FBS (Thermo Fisher Scientific) plus 1 mg/mL aminocaproic acid (Millipore Sigma) was pipetted through the cavity from the displaced wire or O-ring. The microfluidic device was cultured at 37°C to allow the gelled thrombin to further diffuse into the cell-fibrinogen solution to form a fibrin-muscle strip. After 30 min at 37°C, the gelatin solution was replaced with cell media treated with of 5 μM ROCK inhibitor (Tocris). Media was replaced daily from the center well.

3.4 | Image processing

Although fluorescent staining of cytoskeletal actin is typically used to quantify cell alignment,[5] high resolution brightfield images (Supplemental Data S1) can also generate comparable data as previously shown.[42] Here, images were processed using a custom MATLAB (MathWorks, Inc) script. High resolution brightfield images were analyzed by first transforming the images into 8-bit representations. A 2-by-2 median filtering *Medfilt2* operation was applied to ensure proper identification of edges. Brightfield images were smoothed and then enhanced by increasing the image brightness and contrast (Supplemental Data S2A). Image threshold values, optimized for each image, were then tuned into binary images using *Graythresh* and *Shanbhag* thresholding (Supplemental Data S2B). The *Watershed* feature was used to isolate individual cells.

3.5 | Quantification of cell alignment and elongation

Rose diagrams were generated in MATLAB using data collected from Fiji's analyze particles function. All orientations were normalized to

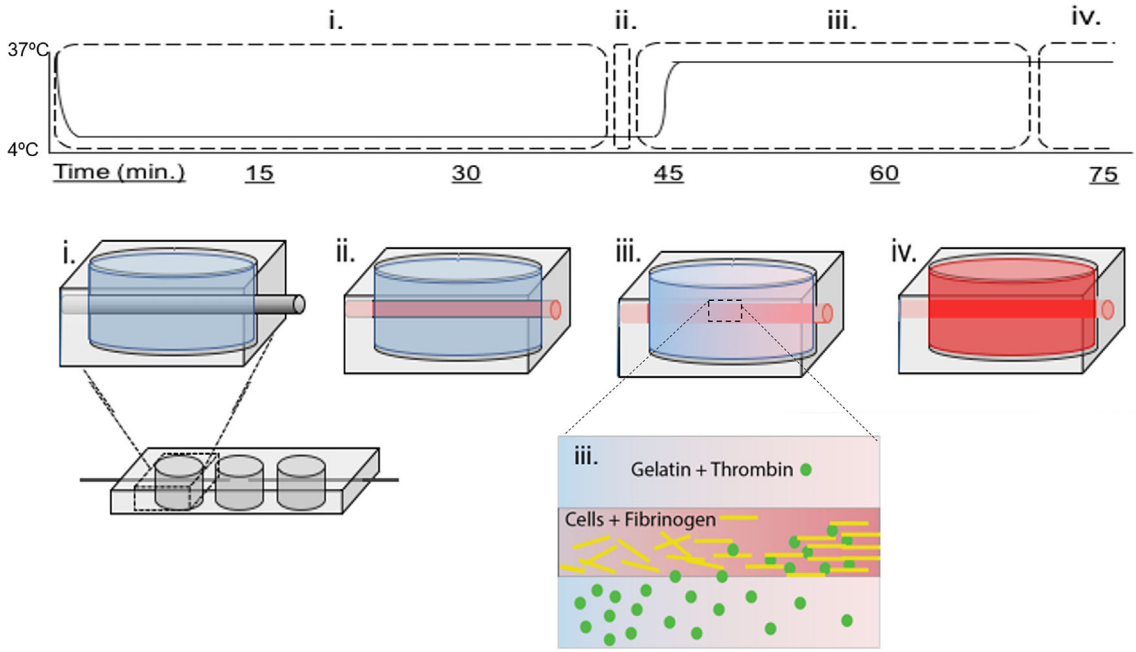

FIGURE 3 Fabrication of 3D muscle strips. (i) Muscle strip formation starts with pipetting a solution of gelatin and thrombin over music wire in the outer well(s) of the microfluidic device. (ii) Once the gel solidifies, the music wire is replaced with a cell-fibrinogen solution, and (iii) placed in the incubator. The warmer temperature returns the gel to a liquid state, allowing the thrombin to diffuse into the lumen with the cell-fibrinogen solution and forms a fibrin gel with the embedded cells. (iv) After approximately 25 min, the liquid gelatin is replaced with cell culture medium.

reflect a 0°–90° measurement and plotted on a 0°–90° polar histogram (polarhistogram). The plotted bin size was set to 6°. The mean angle was also calculated and displayed in text. Binary actin lengths between 10 and 200 pixels were measured. Anything smaller or larger was assumed to be an image artifact. The percentage of aligned cells was defined as any cell between ±30° from the wrinkle or average direction on a flat surface. The elongation factor (EF) was calculated using a ratio of each cell's maximal diameter (D_{max}), length, to the minimal diameter (D_{min}), width.

$$EF = D_{max}/D_{min} \quad (1)$$

3.6 | Statistical analysis

All comparisons for statistical significance were conducted using a student's *t*-test using the mean degree of alignment or EF, and the standard deviation for $N = 100$ cells.

4 | RESULTS

4.1 | Cell characterization

The hiPSCs were cultured at least 2 weeks before differentiating into the cardiac cells with verified expression of pluripotent marker Oct ¾ (Figure 4) and healthy colony formation verified prior to induction. After induction and purification of the CMs, the CMs expressed functional sarcomeric α-actinin z-bands (Figure 5A). Purification was achieved with 92% cardiac troponin-T+ cells (Figure 5B). The spontaneous contraction rates of the CMs exhibit two distinct sets of spontaneously contracting cells beating either ∼70 bpm or ∼ 110 bpm (Figure 5C), likely corresponding with nodal CMs and atrium-like CMs, respectively.[43] No differences were observed between single cells, or clusters with 5 or more cells together.

4.2 | Fabrication of 3D muscle

All three protocols successfully generated compacted tissue comprised of hiPSC-derived CMs (Figure 6A–C). Once the 3D tissue assembly methods were found to be reproducible and maintained structural integrity for at least 2 weeks, the alignment and cell elongation of the hiPSC-derived CMs was evaluated. The cardiospheres formed into raised disk-shapes rather than spheres with little cell alignment and no elongation. The percentage of aligned cells was greatest in the muscle strip (55%) and the muscle ring (50%) compared with the relatively unaligned cardiospheres (35%) (Figure 6E). The iPSC-derived CMs within the muscle strip also exhibited the greatest elongation, with elongation factor at 2.0 compared with 1.5 for the muscle ring and 1.2 for the cardiospheres.

5 | DISCUSSION AND CONCLUSIONS

Protocols for differentiating human ESC and iPS cells into CMs typically contain mixtures of ventricular-like, atrial-like, and nodal-like CMs.[44] The human iPSC-derived CMs used in these studies exhibited

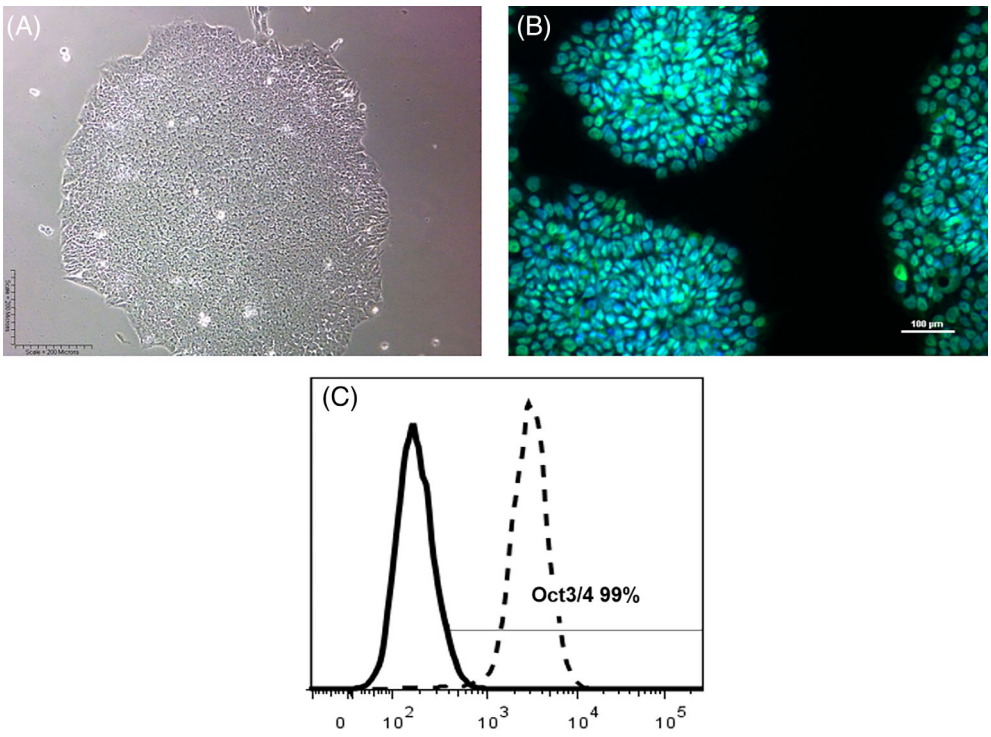

FIGURE 4 Characterization of the DF19-9-7 T human iPSCs. (A) Bright field image of the human iPSC colony taken at a 20× magnification (scale bar 200 µm). (B) Fluorescent image of the hiPSC colonies stained with Oct3/4 (green) and counterstained with DAPI (blue). Scale bar 100 µm. (C) Histogram of flow cytometry data showing the percentage of cells expressing pluripotent stem cell markers Oct-3/4.

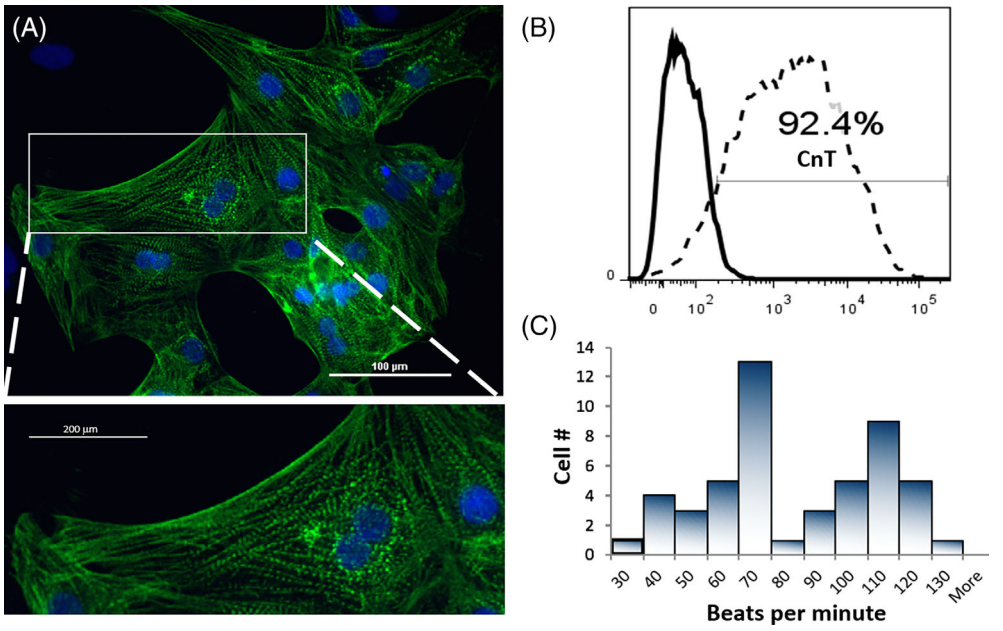

FIGURE 5 Characterization of human iPSC-derived CMs. (A) Differentiated CMs are stained with α-actinin (green) and counterstained with DAPI nuclear stain (blue). Scale bar = 100 μm. The α-actinin staining shows the striations of *z*-bands in the myofibrils. (B) Histogram showing the percentage of human iPSC-derived CMs expressing cardiac troponin. (C) Contracting human iPSC-derived CMs ($n = 100$) were analyzed for rates of contraction. Most cells contract at 70 beats per minute, with a second group of cells contracting at a faster pace.

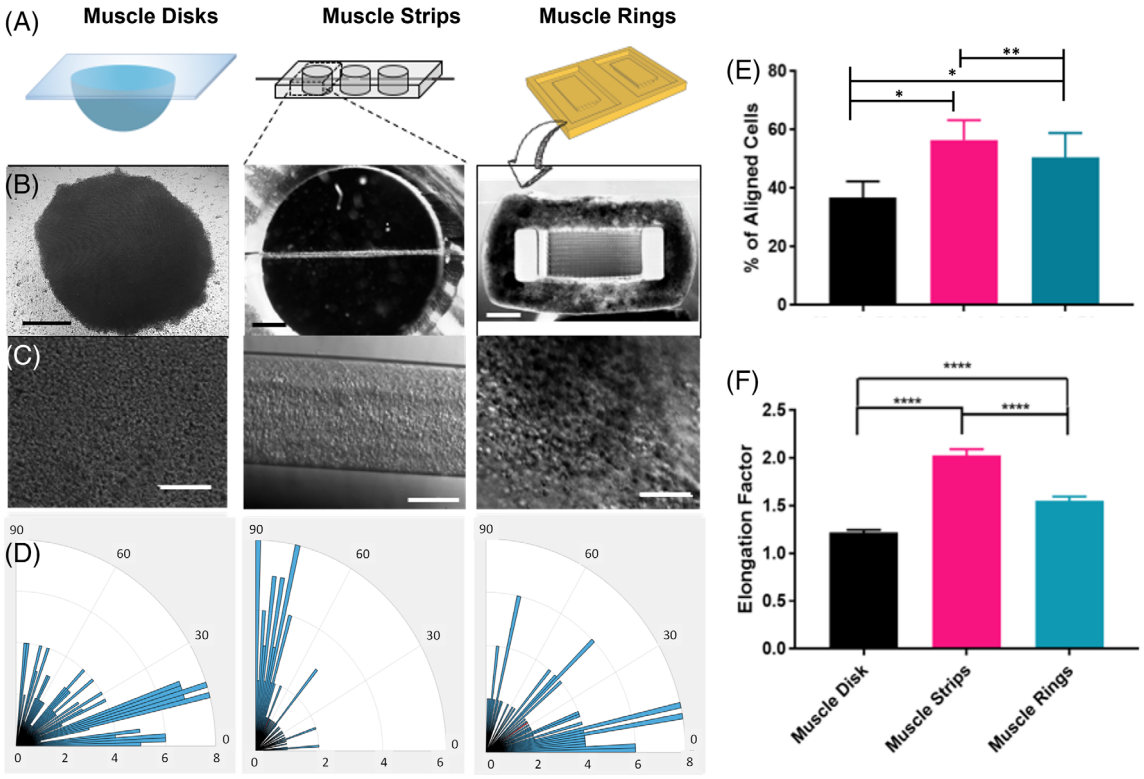

FIGURE 6 Alignment of 3D CM tissue. (A) Schematic representations of 3D muscle tissue formed as cardiospheres (i.e. muscle disks), muscle strips, and muscle rings. Stitched brightfield images were taken at (B) low magnification, scale bar = 1000 μm, and (C) higher magnification, scale bar = 100 μm. (D) Rose-plots showing individual cell orientations with respect to the primary direction for each tissue. (E) The percentage of aligned hiPSC-derived CMs within the three different tissues was calculated $^{*}p < .0001$ and $^{**}p < .02$. (F) The elongation factor calculated for the hiPSC-derived CMs within the three different tissues. $^{***}p < .0001$.

beating rates at ~70 and ~ 110 bpm, respectively, correlating with atrial-like and nodal-like,[43] with spontaneous beating of CMs suggesting that these cells are more fetal-like than less spontaneously contracting mature cardiac cells.[45] Studies exploring extended culture times, electrical pacing, mechanical stretch, or pharmacological agents aim to increase the maturity of iPSC-CMs (reviewed in[46]).

Here we show that muscle strip and ring methods of cardiac tissue fabrication both generate aligned CMs from hiPSC-derived CMs.

TABLE 1 Summary: Table summarizing each fabrication method, corresponding alignment, and expected contractile forces.

	Cell concentration (million/mL)	% of aligned cells	Elongation factor	Scalability	Contractile force generation
Muscle disks	20	35%	1.2	Highly	0.25 mN/mm^2
Muscle rings	10	50%	1.5	Minimally	*
Muscle strips	20	55%	2.0	Somewhat	0.55 mN/mm^2
Native tissue	100–1000	~100%	4.3 (rat)	N/A	25–44 mN/mm^2

*not available

Consistent with previous studies using skeletal C2C12s[47–49] the muscle strip was superior in generating a greater percentage of aligned cells with a larger elongation factor (summarized in Table 1). The alignment and elongation factors are of interest because these have been shown to correlate strongly with muscle tissues' ability to generate and sustain high contractile forces critical for generating large ejection fractions during heart contractions.[50] The elongated shape of CMs correlates with the shape and organization of the sarcomere, an important mechanism by which the heart regulates its force of contraction, and the CMs actin networks and organized sarcomere arrays is regulated by its shape.[51] With increased sarcomere length, there is an increase in the force of contraction (i.e., tension development by the muscle fiber). Well-organized cardiac monolayers can be as much as 2× the force measured in isotropic tissues.[17] Several groups have shown the CM cell alignment and elongation can be achieved using micropatterning,[5,17,52,53] but this is proving more difficult in 3D tissue. The superior elongation found in the muscle strips compared with disks or rings (Table 1) is likely due to the ability of those tissues to generate greater tensions from the biaxial attachments at the ends of the muscle strips.

Although tissue contraction is the gold standard for measuring heart tissue function, comparing the contractile forces of 3D cardiac tissue is complicated by the various tissue shapes and thicknesses, as well as, various methods used to calculate muscle cell and tissue contractile forces, and most reported values do not average the contractile forces over the tissue area. Here, we also provide reported values for 3D cardiac tissues generated from stem cell-derived CMs in units of force per area of tissue (Table 1) after pacing at 2 Hz. Consistent with expectations, unaligned human ESC-derived CM patches exhibit lower contractile forces 0.25 mN/mm^2 of force after 25% strain[54] compared with aligned strips at 0.6 mN/mm^2.[55] This manuscript is the first report of ring-shaped tissue generated from hiPS-CMs, but mature rat neonatal cardiac cells patterned into ring-shaped tissue can generate forces at 2 mN/mm^2 (reported as twitch tension).[24] To date, the best stem cell-derived 3D cardiac tissues generated in vitro exhibits forces almost two orders of magnitude lower than native myocardium which can generate 25 mN/mm^2 of contractile forces at rest and up to 45 mN/mm^2 at maximal output.[56]

Conduction velocities (CVs) of CMs are another indicator of heart function. CVs measure the speed of conduction of an electrical impulse through the cells or tissue. The conduction velocity of aligned monolayers of genetically purified induced CMs has been reported as high as ~21 cm/s,[57] with more complex 3D systems at 17 cm/s[58] and up to 25 cm/s when highly organized.[59] Again, these values still fall short of CVs in native adult tissue ~30 to 100 cm/s.[60] The highest CVs reported for 3D engineered cardiac tissue was obtained using neonatal rat CMs at 32 cm/s,[61] rather than from immature stem cell-derived CMs.

One of the primary limitations in current fabrication methods for generating cardiac muscle tissue is the cell density. The cell density of native myocardium in rats is between 50 and 100 million cells per mL[62] and 100–1000 million cells per mL in humans.[63] However, current methods are not yet able to incorporate more than 20 million viable CMs per mL into hydrogels, likely contributing to the lower contractile forces. This limitation may also be related to the limits of oxygen diffusion in current engineered tissue. An in vitro model at 20 million cells per mL cannot be thicker than a few 100 μm, otherwise a necrotic core will develop. At higher cell densities, the viability of the cells will only decrease without a network of perfused capillaries. In fact, the metabolic activity of cardiac cells is so high that a ratio of three endothelial cells to one cardiomyocyte is usually cited as required.

Current improvements in stem cell derivation methods and engineering cardiac tissue fabrication methods—longer culture times, muscle conditioning (i.e. static or dynamic stretching),[64] electrical signaling[30] or incorporation of cardiac fibroblasts[65,66]—have improved current engineered cardiac muscle by make possible a platform for disease modeling and drug discovery, the use of engineered cardiac tissue for heart tissue repair and, eventually, replacement remains limited by key challenges in cell density and vascular perfusion.

ACKNOWLEDGMENTS

This work was funded through the NSF-Science and Technology Center (STC) for the Emergent Behavior of Integrated Biological Systems (EBICS) Award #0939511.

DATA AVAILABILITY STATEMENT

The data that support the findings of this study are openly available in Open Source Framework at https://osf.io/tgrk5/.

ORCID

Kara E. McCloskey https://orcid.org/0000-0002-4674-3219

REFERENCES

1. Hay M, Thomas DW, Craighead JL, Economides C, Rosenthal J. Clinical development success rates for investigational drugs. *Nat Biotechnol*. 2014;32(1):40-51.
2. Ronaldson-Bouchard K, Vunjak-Novakovic G. Organs-on-a-Chip: A Fast track for engineered human tissues in drug development. *Cell Stem Cell*. 2018;22(3):310-324.

3. Shi Y, Inoue H, Wu JC, Yamanaka S. Induced pluripotent stem cell technology: a decade of progress. *Nat Rev Drug Discov*. 2017;16(2):115-130.
4. Huang S, Ingber DE. Shape-dependent control of cell growth, differentiation, and apoptosis: switching between attractors in cell regulatory networks. *Exp Cell Res*. 2000;261(1):91-103.
5. Luna JI, Ciriza J, Garcia-Ojeda ME, et al. Multiscale biomimetic topography for the alignment of neonatal and embryonic stem cell-derived heart cells. *Tissue Eng Part C Methods*. 2011;17(5):579-588.
6. Van Essen D, Kelly J. Correlation of cell shape and function in the visual cortex of the cat. *Nature*. 1973;241(5389):403-405.
7. Huet C, Pisselet C, Mandon-Pepin B, Monget P, Monniaux D. Extracellular matrix regulates ovine granulosa cell survival, proliferation and steroidogenesis: relationships between cell shape and function. *J Endocrinol*. 2001;169(2):347-360.
8. Haeuptle MT, Suard YL, Bogenmann E, Reggio H, Racine L, Kraehenbuhl JP. Effect of cell shape change on the function and differentiation of rabbit mammary cells in culture. *J Cell Biol*. 1983;96(5):1425-1434.
9. Kumar G, Tison CK, Chatterjee K, et al. The determination of stem cell fate by 3D scaffold structures through the control of cell shape. *Biomaterials*. 2011;32(35):9188-9196.
10. Kuo PL, Lee H, Bray MA, et al. Myocyte shape regulates lateral registry of sarcomeres and contractility. *Am J Pathol*. 2012;181(6):2030-2037.
11. Jalili-Firoozinezhad S, Prantil-Baun R, Jiang A, et al. Modeling radiation injury-induced cell death and countermeasure drug responses in a human gut-on-a-Chip. *Cell Death Dis*. 2018;9(2):223.
12. Ma W, Fitzgerald W, Liu QY, et al. CNS stem and progenitor cell differentiation into functional neuronal circuits in three-dimensional collagen gels. *Exp Neurol*. 2004;190(2):276-288.
13. Chung S, Sudo R, Vickerman V, Zervantonakis IK, Kamm RD. Microfluidic platforms for studies of angiogenesis, cell migration, and cell-cell interactions. Sixth International Bio-Fluid Mechanics Symposium and Workshop March 28–30, 2008. *Ann Biomed Eng*. 2010;38(3):1164-1177.
14. Jung G, Fajardo G, Ribeiro AJS, et al. Time-dependent evolution of functional vs. remodeling signaling in induced pluripotent stem cell-derived cardiomyocytes and induced maturation with biomechanical stimulation. *FASEB J*. 2015;30:1464-1479.
15. Rao C, Prodromakis T, Kolker L, et al. The effect of microgrooved culture substrates on calcium cycling of cardiac myocytes derived from human induced pluripotent stem cells. *Biomaterials*. 2013;34(10):2399-2411.
16. Yin L, Bien H, Entcheva E. Scaffold topography alters intracellular calcium dynamics in cultured cardiomyocyte networks. *Am J Physiol Heart Circ Physiol*. 2004;287(3):H1276-H1285.
17. Feinberg AW, Alford PW, Jin H, et al. Controlling the contractile strength of engineered cardiac muscle by hierarchal tissue architecture. *Biomaterials*. 2012;33(23):5732-5741.
18. Voorhees AP, Han HC. A model to determine the effect of collagen fiber alignment on heart function post myocardial infarction. *Theor Biol Med Model*. 2014;11:6.
19. Shimizu T, Yamato M, Kikuchi A, Okano T. Cell sheet engineering for myocardial tissue reconstruction. *Biomaterials*. 2003;24(13):2309-2316.
20. Sekine H, Shimizu T, Dobashi I, et al. Cardiac cell sheet transplantation improves damaged heart function via superior cell survival in comparison with dissociated cell injection. *Tissue Eng Part A*. 2011;17(23–24):2973-2980.
21. Turner WS, Wang X, Johnson S, et al. Cardiac tissue development for delivery of embryonic stem cell-derived endothelial and cardiac cells in natural matrices. *J Biomed Mater Res B Appl Biomater*. 2012;100(8):2060-2072.
22. Sanchez PL et al. Acellular human heart matrix: a critical step toward whole heart grafts. *Biomaterials*. 2015;61:279-289.
23. Eschenhagen T, Fink C, Remmers U, et al. Three-dimensional reconstitution of embryonic cardiomyocytes in a collagen matrix: a new heart muscle model system. *FASEB J*. 1997;11(8):683-694.
24. Zimmermann WH, Schneiderbanger K, Schubert P, et al. Tissue engineering of a differentiated cardiac muscle construct. *Circ Res*. 2002;90(2):223-230.
25. Lange WJd et al. Neonatal mouse–derived engineered cardiac tissue. *Circ Res*. 2011;109(1):8-19.
26. Hansen A, Eder A, Bönstrup M, et al. Development of a drug screening platform based on engineered heart tissue. *Circ Res*. 2010;107(1):35-44.
27. Ma SP, Vunjak-Novakovic G. Tissue-engineering for the study of cardiac biomechanics. *J Biomech Eng*. 2016;138(2):021010.
28. Chan V, Raman R, Cvetkovic C, Bashir R. Enabling microscale and nanoscale approaches for bioengineered cardiac tissue. *ACS Nano*. 2013;7(3):1830-1837.
29. Aubin H, Nichol JW, Hutson CB, et al. Directed 3D cell alignment and elongation in microengineered hydrogels. *Biomaterials*. 2010;31(27):6941-6951.
30. Nunes SS, Miklas JW, Liu J, et al. Biowire: a platform for maturation of human pluripotent stem cell-derived cardiomyocytes. *Nat Methods*. 2013;10(8):781-787.
31. Chan V, Neal DM, Uzel SGM, Kim H, Bashir R, Asada HH. Fabrication and characterization of optogenetic, multi-strip cardiac muscles. *Lab Chip*. 2015;15(10):2258-2268.
32. Li TS, Cheng K, Lee ST, et al. Cardiospheres recapitulate a niche-like microenvironment rich in stemness and cell-matrix interactions, rationalizing their enhanced functional potency for myocardial repair. *Stem Cells*. 2010;28(11):2088-2098.
33. Davis DR, Ruckdeschel Smith R, Marban E. Human cardiospheres are a source of stem cells with cardiomyogenic potential. *Stem Cells*. 2010;28(5):903-904.
34. Raman R, Cvetkovic C, Uzel SGM, et al. Optogenetic skeletal muscle-powered adaptive biological machines. *Proc Natl Acad Sci U S A*. 2016;113(13):3497-3502.
35. Neal DM et al. Mechanical characterization and shape optimization of fascicle-like 3D skeletal muscle tissues contracted with electrical and optical stimuli. *Tissue Eng Part A*. 2015;21:1848-1858.
36. Ledford HA, Park S, Muir D, et al. Different arrhythmia-associated calmodulin mutations have distinct effects on cardiac SK channel regulation. *J Gen Physiol*. 2020;152(12):1-16.
37. Sirish P, Thai PN, Lee JH, et al. Suppression of inflammation and fibrosis using soluble epoxide hydrolase inhibitors enhances cardiac stem cell-based therapy. *Stem Cells Transl Med*. 2020;9(12):1570-1584.
38. Lian X, Zhang J, Azarin SM, et al. Directed cardiomyocyte differentiation from human pluripotent stem cells by modulating Wnt/beta-catenin signaling under fully defined conditions. *Nat Protoc*. 2013;8(1):162-175.
39. Beauchamp P, Jackson CB, Ozhathil LC, et al. 3D Co-culture of hiPSC-derived cardiomyocytes with cardiac fibroblasts improves tissue-like features of cardiac spheroids. *Front Mol Biosci*. 2020;7:14.
40. Polonchuk L, Chabria M, Badi L, et al. Cardiac spheroids as promising in vitro models to study the human heart microenvironment. *Sci Rep*. 2017;7(1):7005.
41. Cvetkovic C, Raman R, Chan V, et al. Three-dimensionally printed biological machines powered by skeletal muscle. *Proc Natl Acad Sci U S A*. 2014;111(28):10125-10130.
42. Xu F, Beyazoglu T, Hefner E, Gurkan UA, Demirci U. Automated and adaptable quantification of cellular alignment from microscopic images for tissue engineering applications. *Tissue Eng Part C Methods*. 2011;17(6):641-649.

43. Mummery C, Ward-van Oostwaard D, Doevendans P, et al. Differentiation of human embryonic stem cells to cardiomyocytes: role of coculture with visceral endoderm-like cells. *Circulation*. 2003;107(21):2733-2740.
44. Zhang J, Wilson GF, Soerens AG, et al. Functional cardiomyocytes derived from human induced pluripotent stem cells. *Circ Res*. 2009;104(4):e30-e41.
45. Satin J, Kehat I, Caspi O, et al. Mechanism of spontaneous excitability in human embryonic stem cell derived cardiomyocytes. *J Physiol*. 2004;559(Pt 2):479-496.
46. Ahmed RE et al. A brief review of current maturation methods for human induced pluripotent stem cells-derived cardiomyocytes. *Front Cell Dev Biol*. 2020;8:178.
47. Neal D, Sakar MS, Ong LLS, Harry Asada H. Formation of elongated fascicle-inspired 3D tissues consisting of high-density, aligned cells using sacrificial outer molding. *Lab Chip*. 2014;14(11):1907-1916.
48. Raman R, Cvetkovic C, Bashir R. A modular approach to the design, fabrication, and characterization of muscle-powered biological machines. *Nat Protoc*. 2017;12(3):519-533.
49. Grant L, Raman R, Cvetkovic C, et al. Long-term cryopreservation and revival of tissue-engineered skeletal muscle. *Tissue Eng Part A*. 2019;25(13–14):1023-1036.
50. Rens EG, Merks RMH. Cell contractility facilitates alignment of cells and tissues to static uniaxial stretch. *Biophys J*. 2017;112(4):755-766.
51. Bray MA, Sheehy SP, Parker KK. Sarcomere alignment is regulated by myocyte shape. *Cell Motil Cytoskeleton*. 2008;65(8):641-651.
52. Agarwal A, Farouz Y, Nesmith AP, Deravi LF, McCain ML, Parker KK. Micropatterning alginate substrates for cardiovascular muscle on a Chip. *Adv Funct Mater*. 2013;23(30):3738-3746.
53. Bursac N, Parker KK, Iravanian S, Tung L. Cardiomyocyte cultures with controlled macroscopic anisotropy: a model for functional electrophysiological studies of cardiac muscle. *Circ Res*. 2002;91(12):e45-e54.
54. Stevens KR, Kreutziger KL, Dupras SK, et al. Physiological function and transplantation of scaffold-free and vascularized human cardiac muscle tissue. *Proc Natl Acad Sci U S A*. 2009;106(39):16568-16573.
55. Nakane T, Masumoto H, Tinney JP, et al. Impact of cell composition and geometry on human induced pluripotent stem cells-derived engineered cardiac tissue. *Sci Rep*. 2017;7(1):45641.
56. Mulieri LA, Hasenfuss G, Leavitt B, Allen PD, Alpert NR. Altered myocardial force-frequency relation in human heart failure. *Circulation*. 1992;85(5):1743-1750.
57. Lee P, Klos M, Bollensdorff C, et al. Simultaneous voltage and calcium mapping of genetically purified human induced pluripotent stem cell-derived cardiac myocyte monolayers. *Circ Res*. 2012;110(12):1556-1563.
58. Pretorius D, Kahn-Krell AM, LaBarge WC, et al. Fabrication and characterization of a thick, viable bi-layered stem cell-derived surrogate for future myocardial tissue regeneration. *Biomed Mater*. 2021;16(3):35007.
59. Gao L, Kupfer ME, Jung JP, et al. Myocardial tissue engineering with cells derived from human-induced pluripotent stem cells and a native-like, high-resolution, 3-dimensionally printed scaffold. *Circ Res*. 2017;120(8):1318-1325.
60. Yang X, Pabon L, Murry CE. Engineering adolescence: maturation of human pluripotent stem cell–derived cardiomyocytes. *Circ Res*. 2014;114(3):511-523.
61. Jackman CP, Ganapathi AM, Asfour H, et al. Engineered cardiac tissue patch maintains structural and electrical properties after epicardial implantation. *Biomaterials*. 2018;159:48-58.
62. Radisic M, Euloth M, Yang L, Langer R, Freed LE, Vunjak-Novakovic G. High-density seeding of myocyte cells for cardiac tissue engineering. *Biotechnol Bioeng*. 2003;82(4):403-414.
63. Serpooshan V, Chen P, Wu H, et al. Bioacoustic-enabled patterning of human iPSC-derived cardiomyocytes into 3D cardiac tissue. *Biomaterials*. 2017;131:47-57.
64. Tulloch NL, Muskheli V, Razumova MV, et al. Growth of engineered human myocardium with mechanical loading and vascular coculture. *Circ Res*. 2011;109(1):47-59.
65. Li Y, Asfour H, Bursac N. Age-dependent functional crosstalk between cardiac fibroblasts and cardiomyocytes in a 3D engineered cardiac tissue. *Acta Biomater*. 2017;55:120-130.
66. Zhang D, Shadrin IY, Lam J, Xian HQ, Snodgrass HR, Bursac N. Tissue-engineered cardiac patch for advanced functional maturation of human ESC-derived cardiomyocytes. *Biomaterials*. 2013;34(23):5813-5820.

SUPPORTING INFORMATION

Additional supporting information can be found online in the Supporting Information section at the end of this article.

How to cite this article: Hatano R, Smith AM, Raman R, Zamora JE, Bashir R, McCloskey KE. Comparing fabrication techniques for engineered cardiac tissue. *J Biomed Mater Res*. 2024;1-9. doi:10.1002/jbm.a.37737